Journal of Applied Polymer Science

Evaluation of Photovoltaic Efficiency of Dye-Sensitized Solar Cells Fabricated with Electrospun PVDF-PAN-Fe_2O_3 Composite Membrane

Malaisamy Sethupathy, Priyanka Pandey, Paramasivam Manisankar
Department of Industrial Chemistry, Alagappa University, Karaikudi 630003, Tamil Nadu, India
Correspondence to: P. Manisankar (E-mail: pms11@rediffmail.com)

ABSTRACT: Poly(vinylidene fluoride)-polyacrylonitrile-based membranes containing Fe_2O_3 nanoparticles were prepared by electrospinning technique and characterized by HR-SEM, FTIR, and XRD analysis. The effect of electrolyte in the electrospun nanofibers on electrolyte uptake, ionic conductivity and porosity were studied. The electrospun membranes containing Fe_2O_3 showed an enhanced ionic conductivity than that of without Fe_2O_3. Among the prepared membranes, the membrane with 7 wt % Fe_2O_3 has the highest liquid electrolyte uptake of 562% and ionic conductivity of 6.81×10^{-2} S cm^{-1}. The photovoltaic performance for open circuit voltage (V_{oc}), Short-circuit current density (J_{sc}), Fill factor (FF), and η of the DSSC fabricated with 7 wt % Fe_2O_3 are 0.77 V, 10.4 mA/cm^2, 0.62 and 4.9%, respectively. © 2014 Wiley Periodicals, Inc. J. Appl. Polym. Sci. **2014**, *131*, 41107.

KEYWORDS: copolymers; electrospinning; fibers; optical and photovoltaic applications; polyelectrolytes

Received 1 March 2014; accepted 4 June 2014
DOI: 10.1002/app.41107

INTRODUCTION

Dye-sensitized solar cells (DSSCs) using organic liquid electrolytes have been received a great attention because of their low fabrication cost, simple structure, and high power conversion efficiency.[1–5] Gratzel et al. have reported a power conversion efficiency of 10.4% for DSSC fabricated using ruthenium complex dye, liquid electrolytes, and Pt counter electrode.[6] However, the problem encountered in the usage of DSSCs using liquid electrolyte is less long-term stability due to the volatility of the electrolyte containing organic solvent. Durability is a fundamental component in the process of commercialization. Then, gel electrolytes are being investigated to alternate the liquid electrolytes.[7–10] One of the way to make a gel electrolyte is to add organic or inorganic (or both) materials. In the past decades, several studies have been carried out on this kind of gel electrolyte and attempted to get great improvements.[11,12] The disadvantages of them are leakage of electrolytes, limited internal shorting and noncombustible reaction products at the electrode surface.[13,14] Development of the newer attention in quasi-solid state DSSCs that employ polymer gel electrolytes, owing to their nonflammable nature, negligible vapor pressure, good permeability into the mesoporous TiO_2, and high ionic conductivity.[15,16] Polymer gel electrolytes such as poly-(acrylonitrile),[17,18] poly(ethylene glycol),[19,20] poly(methylmethacrylate),[21,22] and poly(oligoethylene gylcol methacylate)[23] with different plasticizers have been employed in quasi-solid-state DSSCs. Although DSSCs composed of polymer gel electrolytes do not suffer from electrolyte loss problems, they have low photo conversion efficiency because of the lower electron injection efficiencies of the electrolyte material. However, because of their complex preparing technology and poor mechanical strength, they cannot be used for production.[24,25] To overcome this problem, the polymer membrane is sopping in an electrolyte solution and that has been examined.[26,27]

To prepare the polymer membrane for polymer electrolyte, a number of processing techniques are existing such as drawing,[28] template synthesis,[29,30] phase separation,[31] electrospinning,[32] etc. Among them, the electrospinning technology is a simple and low-cost method for making ultra-thin fibers. This technique makes use of an electrical field that is applied across a polymer solution and a collector, to force a polymer solution jet out from a small hole.[33] When the diameters of polymer fiber materials are shrunk from micrometers to submicrons or nanometers, several amazing characteristics appear such as a very large surface area to volume ratio, flexibility in surface functionalities, and superior mechanical performances compared with any other known forms of this material.[34] In the past decade, electrospinning method has gained greater attention and a vital role. Materials such as synthetic and natural polymer solutions were prepared with electrospun fibers and poly(ethylene oxide) (PEO) in distilled water,[35] polyurethane in *N,N*-dimethylformamide (DMF),[36] poly(ε-caprolactone) (PCL) in acetone,[37] PVDF

Additional Supporting Information may be found in the online version of this article.

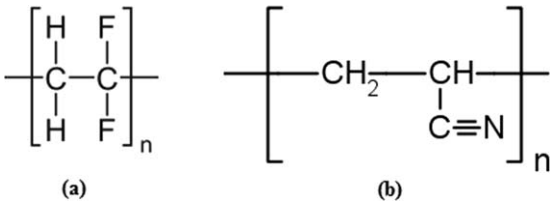

Figure 1. Chemical structure of (a) PVDF (b) PAN.

in acetone/*N,N*-dimethylacetamide (DMAc) (7 : 3 by weight),[38] and regenerated cellulose in 2 : 1 (w/w) acetone/DMAc.[39]

Inorganic metal oxide nanoparticles like alumina (Al_2O_3), zirconium dioxide (ZrO_2), titanium dioxide (TiO_2), silica (SiO_2), and some small molecules of lithium salts[40–44] have been used in the preparation of composite polymer electrolytes. These inorganic nanoparticles improve the mechanical properties, interfacial stability between polymer electrolytes and also to enhance the ionic conductivity by dropping the crystallinity nature of the host polymer and introduce Lewis acid–base interaction between the polar groups of the metal oxide nanoparticles and the electrolyte ionic species.[45] Incorporation of some metal oxides in the polymer electrolyte would improve the photovoltaic efficiency of DSSCs significantly.[46–48]

Since hematite, a thermodynamically stable phase of Fe_2O_3, is a potential candidate for many optical applications, such as solar energy conversion, electrochromism, photocatalysis, interference filters, and photo-oxidation of water.[49–52] The focus of this work lies on the utilization of Fe_2O_3. In this present investigation, we prepared the electrospun PVDF-PAN-Fe_2O_3 composite fibrous membranes and their behavior such as the porosity, electrolyte uptake, conductivity, and morphological characteristics, crystallainity of polymer composite electrolyte were found out. We have used a new approach to enhance the performance of the polymer electrolyte which is useful to increase the efficiency of the DSSC (Figure 1).

EXPERIMENTAL

Materials

Poly(vinylidene fluoride) (PVDF), Polyacrylonitrile (PAN), Iron oxide (Fe_2O_3), acetone, *N,N*-dimethylacetamide, lithium iodide, iodine, ethylene carbonate (EC), propylene carbonate (PC), 1-Hexyl-2,3-dimethylimidazolium iodide were purchased from Aldrich Chemicals and 4-*tert*-butylpyridine from TCI Chemicals. All reagents were used without further purification and other reagents and solvents were commercially available and they were used as received.

Preparation of Electrospun Nanofiber Composite Membrane PVDF-PAN-Fe_2O_3

Mixture of PVDF-PAN solution was prepared by dissolving a mixture of PVDF and PAN in 3 : 1 weight ratio in acetone : DMF (7 : 3 v/v). Then different quantities of Fe_2O_3 were mixed at 60°C for 12 h. The contents of Fe_2O_3 in the composite were 0, 3, 5, and 7 wt % based on the weight of PVDF-PAN.[53] Further, the composite blend solution was filled in to a 10 mL stainless steel syringe (needle-24 G) using a syringe pump (KD Scientific, model 100), with a mass flow rate of 1.5 mL h^{-1} and then the steel needle was connected to an electrode. High voltage supply of 20 kV was applied to the end of the needle. The distance between the syringe nozzle and the aluminum foil collector was kept at 15 cm at room temperature. Electrospinning was started and after the completion of the process, the nanofibrous membrane was carefully peeled off from the aluminium foil. The collected membranes were vacuum dried at 80°C for 12 h.

Characterization of Elecrospun Nanofiber Composite Membrane (PVDF-PAN-Fe_2O_3)

Morphology Observation. The morphology of composite membranes was examined by a high resolution scanning electron microscopy (HRSEM) (FEI Quanta 250 Microscope, Netherland). The average diameter of the nanofibers was determined by analyzing the HRSEM images with an image analyzing software (Gwyddion 2.28).

X-ray Diffraction (XRD) and Fourier Transform Infrared (FTIR) Analysis

The XRD measurement was carried out to analyze the crystalline phase of PVDF–PAN-Fe_2O_3 nanofiber membranes which were evaluated by computer controlled XRD system ("X" Pert PRO PAN anlytical diffractometer) with Cu Kα radiation at 40 kV/30 mA. The diffractograms were scanned in a 2θ range of 10–70 at a rate of 2 min^{-1}.

Fourier transform infrared (FTIR) spectra was recorded using KBr pellet using Nicolet 5700 spectrophotometer (Thermo Electron Co., USA) in the wave number range of 400–4000 cm^{-1} to determine the presence of functional groups in PVDF-PAN-Fe_2O_3 electrospun nanofiber membrane.

Porosity Measurements. The membrane porosity ε (%) was defined as the volume of the pores divided by the total volume of the porous membrane. It could usually be determined by gravimetric method, determining the weight of liquid contained in the membrane pores.[54] The porosity percentage of PVDF-PAN-Fe_2O_3 composite electrospun membrane was determined using n-butanol uptake. For this purpose composite membrane was soaked in n-butanol for 2 h. The mass of PVDF-PAN-Fe_2O_3 composites membrane before and after immersion was measured. The porosity % of the membrane was calculated using the eq. (1):[55]

$$\varepsilon(\%) = \frac{(w_1 - w_2)/d_b}{(w_1 - w_2)/d_b + w_2/d_p} \times 100 \quad (1)$$

Where w_1 is the weight of the wet membrane (g), w_2 is the weight of the dry membrane (g), after and before soaking in n-butanol, whereas d_b and d_p were density of the n-butanol, and polymer respectively.

Electrolyte Uptake Measurements. To determine the electrolyte uptake of the composite PVDF-PAN-Fe_2O_3 electrospun nanofiber, it was soaked in an electrolyte solution containing 0.6*M* 1-hexyl-2,3-dimethylimidazolium iodide, 0.1*M* LiI, 0.05*M* I_2, and 0.5*M* 4-*tert*-butylpyridine in EC/PC (1 : 1 wt %).[56–58] The % of electrolyte uptake of the electrospun membrane was determined by soaking the membranes in liquid electrolyte solution and determined at various soaking interval. The initial weight

of the dried and wetted composite membranes was measured. After that, the membranes were soaked in liquid electrolytes. Then, they have taken out. For the removal of excess electrolyte, a nonwoven tissue paper was used. The electrolyte uptake was calculated using the eq. (2).[59]

$$\text{Electrolyte uptake}(\%) = \frac{M_{wet} - M_{dry}}{M_{dry}} \times 100\% \quad (2)$$

where, M_{wet} and M_{dry} are mass of membranes after and before soaking in the liquid electrolyte, respectively.

Impedance Study. The ionic conductivity was calculated using the Frequency response analyser (FRA) (Autolab PGSTAT 30, Netherlands) by scanning from 10 mHz to 100 kHz. The electrospun PVDF-PAN-Fe_2O_3 composite membranes were immersed in liquid electrolyte solution consisting of 0.6*M* 1-hexyl-2,3-dimethylimidazolium iodide, 0.1*M* LiI, 0.05*M* I_2, and 0.5*M* 4-*tert*-butylpyridine in EC/PC (1 : 1 volume %) for 60 min. During the measurement, the electrolyte samples were sandwiched between two stainless steel (SS) blocking electrodes (surface area : 1 cm^2). Using an FRA1260 frequency response detector, the resistance of the polymer electrolyte was measured. The frequency ranged from 10 mHz to 5 MHz and the ac amplitude was 10 mV at room temperature. The data was analyzed by Z-plot software. The bulk resistance of the polymer electrolyte was determined from the Impedance spectrum. Afterwards, the ionic conductivity was obtained using the following eq. (3):[56]

$$\sigma = \frac{d}{R_b S} \quad (3)$$

Here, σ is the ionic conductivity, R_b is the bulk resistance and d and S are the thickness and surface area of the specimen, respectively.

Contact Angle Measurements

To understand the wettability of PVDF-PAN nanofiber membrane and its composite with Fe_2O_3 nanoparticles, the contact angle was measured using VCA optima, ACT product, INC. Hydrophilic or hydrophobic characteristics of samples were predictable by contact angle (θ) value. The wetting liquid was Milli-pore-grade distilled water (liquid surface tension ($\gamma 1$) = 72.8 mJ m^{-2}).[60] A portion of membrane was placed on a platform and deionized (DI) water was used as liquid at room temperature. A micro-syringe was then used to generate the droplets (5 μL) on the membrane surface. The instrument captures a digital image of the drop on the membrane and estimates the θ by geometrical methods (sessile drop, circle-fitting, etc.) When a drop of liquid is brought into contact with a flat solid surface, the final shape taken by the drop is expressed by "θ". To reduce experimental error, the contact angles were calculated three times for all samples and then averaged. The increased value of cosθ denoted the higher wettability characteristics of the material.

Fabrication of DSSC Devices

The fabrication of DSSC device involved with the incorporation of working electrode (TiO_2) impregnated with dyes and Pt counter-electrode. To prepare the working electrode, a thin layer of nonporous TiO_2 film was deposited on cleaned FTO conducting substrate using 5% titanium (IV) butoxide in ethanol by spin-coating at 3000 rpm. The TiO_2 paste spread on the conducting glass substrate using a doctor blade technique followed by annealing at 450°C. Furthermore, for the preparation of dye solution, the sensitizer N719 dye was dissolved in 0.3 m*M* of pure ethanol solution and then the TiO_2 film was dipped in the same solvent at room temperature for 24 h. To minimize the moisture of TiO_2 it was exposed to the ambient air, later the dye-sensitized TiO_2 electrode was rinsed with anhydrous ethanol and dried in moisture free air. Simultaneously, counter electrode was prepared using a drop of 5 m*M* chloroplatinic acid (H_2PtCl_6) in 2-propanol and it was spread on the FTO glass, sintered at 450°C for 30 min followed by drying and annealing at a controlled heating rate (5°C/min) and then cooled down from 450 to 25°C at a controlled cooling rate (5°C/min). The DSSC was fabricated by sandwiching a piece of electrospun PVDF-PAN-Fe_2O_3 polymer electrolyte between a dye-sensitized TiO_2 working and Pt counter electrode. The edges of the cell were sealed with 1 mm wide strips of 60 μm thick Surlyn, in order to control the thickness of the electrolyte film and to avoid the short-circuiting of the cell. A hot press was used to press together the film electrode and the counter electrode. A drop of the liquid electrolyte solution was introduced into the clamped electrodes through one of two small holes drilled in the counter electrode. The holes were then covered and sealed with small squares of Surlyn strip. The resulting cells had an active area of 0.5 cm × 0.5 cm.

I–V Measurement

The photovoltaic performance of the DSSC devices were measured by using the solar simulator (150 W simulator, PEC-L11, PECCELL), under air mass 1.5 and 100 mW cm^{-2} of the light intensity. The active area of the DSSC devices measured by using a black mask was 0.5 cm^{-2}. The photoelectron-chemical parameters, i.e., the fill factor (FF) and light-to-electricity conversion efficiency (η), were calculated by the following eqs. (4) and (5):

$$FF = \frac{V_{max} \times J_{max}}{V_{oc} \times J_{sc}} \quad (4)$$

$$\eta(\%) = \frac{V_{max} \times J_{max}}{P_{in}} \times 100 = FF = \frac{V_{oc} J_{sc}}{P_{in}} \times 100 \quad (5)$$

where J_{sc} is the short-circuit current density (mA cm^{-2}); V_{oc} is the open-circuit voltage (V); Pin is the incident light power (mW cm^{-2}); and J_{max} (mA cm^{-2}), and V_{max} (V) are the current density and voltage in the *I–V* curves, respectively, at the point of maximum power output.

RESULTS AND DISCUSSION

Surface Morphology of Electrospun PVDF-PAN-Fe_2O_3 Composite Membranes

The SEM images of PVDF-PAN-Fe_2O_3 electrospun composite nanofiber with different Fe_2O_3 contents are presented in Figure 2(a–c). The resulted nanofiber membranes exhibited fully interconnected large pore structure with uniform pore size distribution. It is important to note that there is no bead formation in the nanofibers due to the optimized conditions of the electrospinning. During accumulation of Fe_2O_3 nanoparticles, the

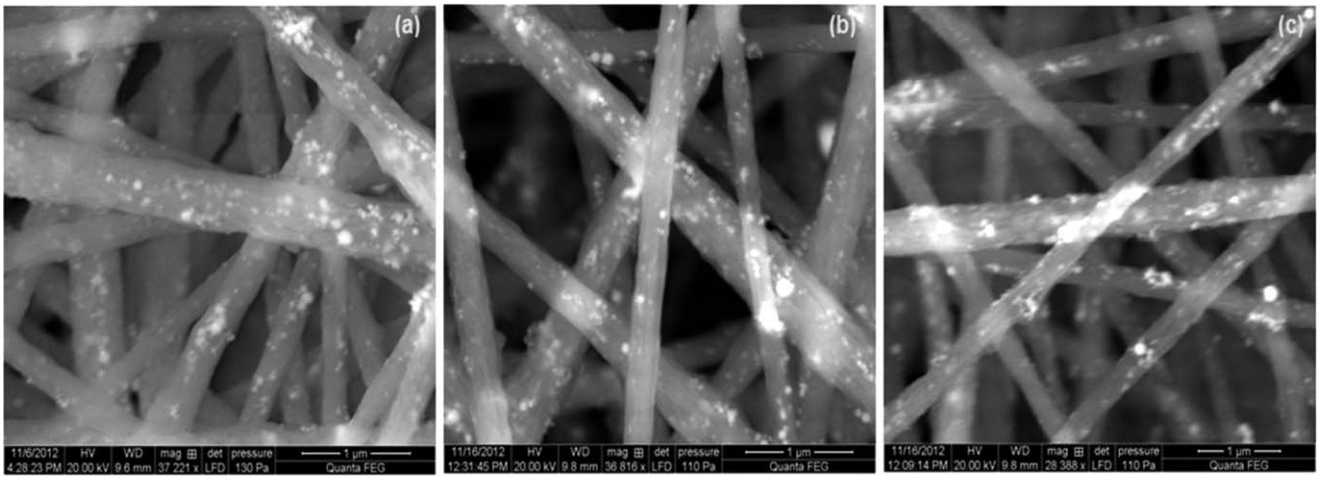

Figure 2. HR-SEM image of electrospun composite nanofiber membranes (a) Fe_2O_3 3 wt %; (b) Fe_2O_3 5 wt %; (c) Fe_2O_3 7 wt %.

surface roughness increased with increasing the Fe_2O_3 contents. The average diameters of composite nanofibers for 3%, 5%, and 7% Fe_2O_3 nanofibers are around 282, 276, and 239 nm, respectively. It is clearly observed that as the Fe_2O_3 content increases, the size of the fiber decreases. This is due to incorporation of higher quantity of Fe_2O_3 which controls the diagonal growth of the fiber. Further increase in the content of Fe_2O_3 resulted in thinning of the fiber which may result in decrease in the strength. The presence of large consistent pores is apparent from the SEM image of electrospun membrane and these results in the high pore volume, which is need for a good membrane.

FTIR Analysis

The FTIR spectrum was recorded for the nanofiber membranes in the range of 400–4000 cm^{-1}. Figure 3(a,b) shows that the peak at about 1403 and 1182 cm^{-1} corresponds to the stretching vibrations of C—F and C—C bonds of PVDF, respectievly. The peaks at 2242, 881, and 442 cm^{-1} are due to the (C—N) stretching vibration, C—F_2 bending mode, and C—F_2 wagging. The peak at 1452 cm^{-1} corresponds to the tensile vibration. The FTIR bands around 564 and 476 cm^{-1} correspond to the Fe—O stretching vibrations.[61] Thus, the FTIR spectral studies revealed that the composite contains PVDF, PAN, and Fe_2O_3.

XRD of Composite Membranes

Figure 4(a–c) shows the XRD pattern of PVDF-PAN-Fe_2O_3 composite membranes with various Fe_2O_3 contents. The XRD results of electrospun PVDF-PAN-Fe_2O_3 membranes exhibited broad peaks at around 20.2°, 20°, and 19.95°, respectively. It suggests that the crystallinity of the composites is decreasing with the increase of Fe_2O_3. Composite with higher percentage of Fe_2O_3 shows more amorphous nature which has been supported by the report of Jung et al.[62] This means that the better dispersion of the Fe_2O_3 nanoparticles to composite solutions enhances the amorphous phase in electrospun composite membranes.

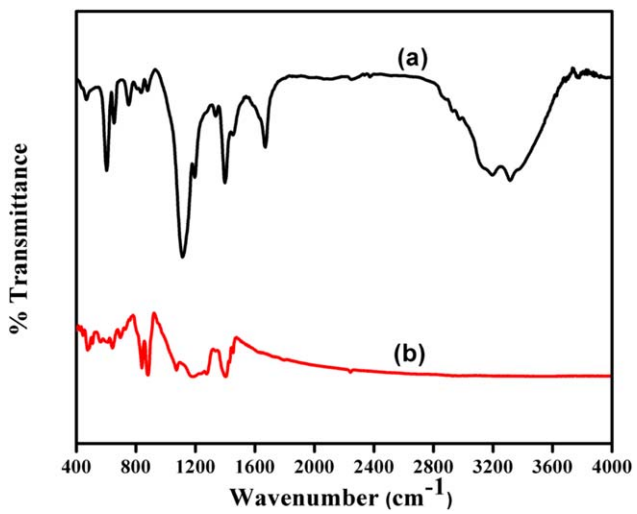

Figure 3. FTIR spectra of (a) PVDF-PAN (b) PVDF-PAN-Fe_2O_3. [Color figure can be viewed in the online issue, which is available at wileyonlinelibrary.com.]

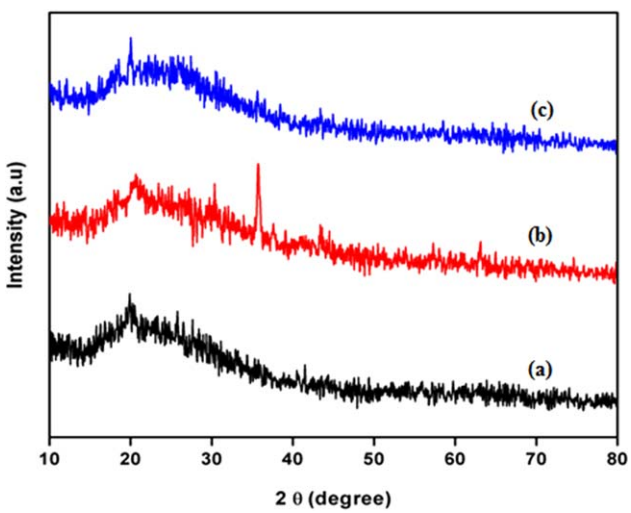

Figure 4. The XRD pattern (a) Fe_2O_3 3 wt %, (b) Fe_2O_3 5 wt %, (c) Fe_2O_3 7 wt %. [Color figure can be viewed in the online issue, which is available at wileyonlinelibrary.com.]

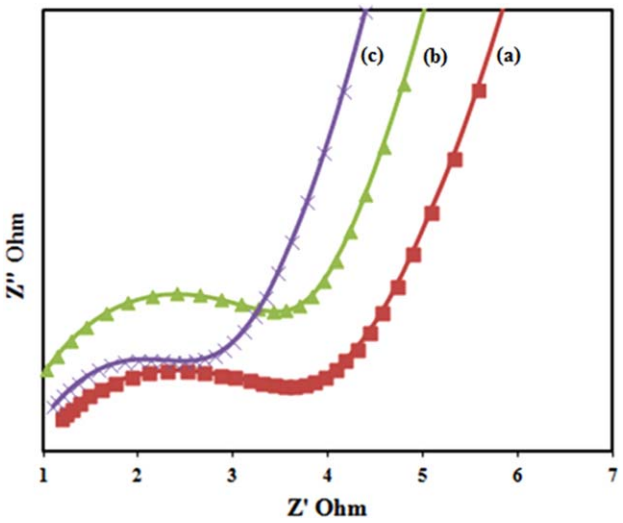

Figure 5. Electrolyte uptake characteristics of (a) Fe_2O_3 3 wt %, (b) Fe_2O_3 5 wt %, (c) Fe_2O_3 7 wt %. [Color figure can be viewed in the online issue, which is available at wileyonlinelibrary.com.]

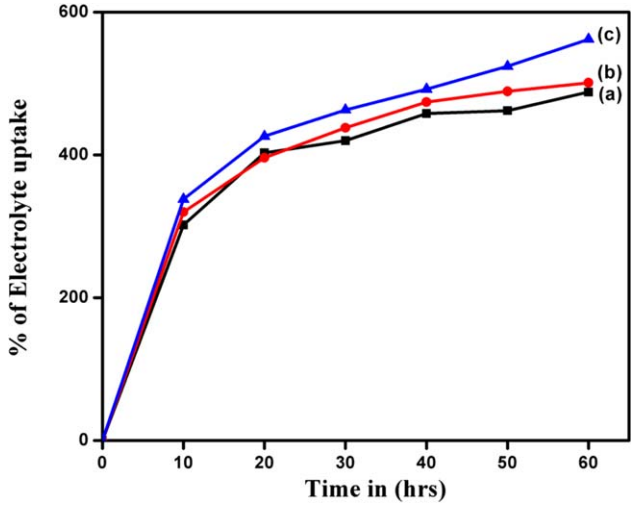

Figure 6. The ionic conductivity of (a) Fe_2O_3 3 wt %, (b) Fe_2O_3 5 wt %, (c) Fe_2O_3 7 wt %. [Color figure can be viewed in the online issue, which is available at wileyonlinelibrary.com.]

Porosity Measurements and Electrolyte Permeation Property

Figure 5(a–c) shows the capacity of electrolyte permeation property and percentage of porosity for electrospun PVDF-PAN-Fe_2O_3 membranes. The average fiber diameter of electrospun membranes playing an important role in determining the membrane porosity, pore size and specific surface area[63] and these parameters are interrelated to the electrolyte uptake of solution, electrochemical performance, and its stability. The electrolyte uptake increase steadily with increasing the Fe_2O_3 concentration in the composite membranes. The electrolyte % uptake of PVDF-PAN-Fe_2O_3 (7%) fiber shows higher uptake of about 562%. Thus, the absorption of the huge amount of liquid electrolyte by the electrospun-composite nanofiber membrane results from higher porosity of the membranes and the higher amorphous content of the polymer. The completely 3D interconnected pore structure makes fast diffusion of the liquid into the membrane and hence the uptake process is alleviated within the initial 10–20 min.

The porosity, measured by n-butyl alcohol (BuOH) uptake, increases from 83.7% to 84.8% with increasing Fe_2O_3 concentration from 3 to 7 wt %. All samples have good porosity due to their well-developed interstices by the interwoven structure among fibers. Composite membrane with 7 wt % Fe_2O_3 shows higher porosity by well-developed large pores/interstices on account of the increased surface roughness. Thus, the membranes with higher degree of porosity enhance the surface area of the pore that result in the higher uptake of the electrolyte solution.

Impedance Study

From the impedance data, the ionic conductivities of the nanofiber membranes at room temperature were calculated. The ionic conductivities of the electrospun–nanofiber membranes were measured at room temperature by the AC impedance method. Figure 6(a–c) shows the AC impedance data of different composition of PVDF-PAN-Fe_2O_3 in polymer electrolytes, respectively. The ionic conductivity mainly depends on the pore structures that catch liquid electrolytes and determined the proper flow of ionic conduction.[64] The ionic conductivities of PVDF-PAN-Fe_2O_3 (3, 5, and 7 wt %) were 6.30×10^{-2} S cm^{-1}, 6.42×10^{-2} S cm^{-1} and 6.81×10^{-2} S cm^{-1}. The higher conductivities are observed due to the well-interwoven structure introduced during electrospinning. Moreover, the incorporation of Fe_2O_3 into the electrospun nanofiber membrane improved the ionic conductivity in the composite. The enhancement of ionic conductivity in composite polymer electrolytes has been attributed mainly to the decreased polymer crystallinity in the presence of the inorganic particles and also to the Lewis acid–base type interactions between the inorganic particles and the electrolyte polar groups.[65]

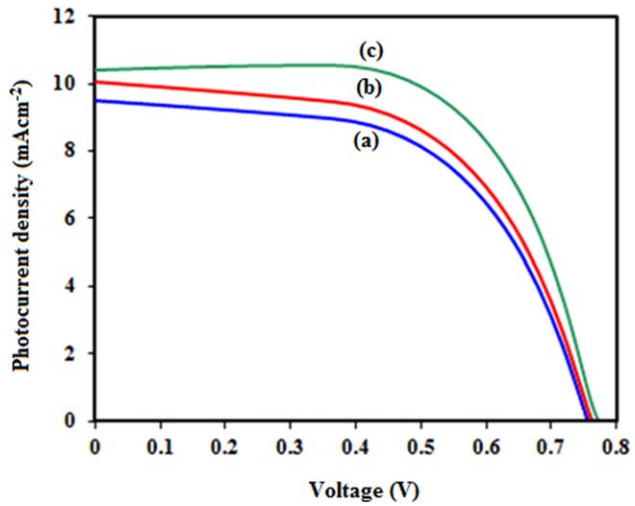

Figure 7. I-V curves of DSSCs using electrospun (a) Fe_2O_3 3wt %; (b) Fe_2O_3 5 wt %; (c) Fe_2O_3 7 wt % nanofiber membrane. [Color figure can be viewed in the online issue, which is available at wileyonlinelibrary.com.]

Table I. Comparison of Photovoltaic Performances of DSSCs Devices Using Electrospun PVDF-PAN-Fe_2O_3 Nanofiber Membrane

Electrolyte	Electrolyte J_{sc} (mA cm^{-2})	V_{oc} (V)	FF	η (%)	Reference
PAN/MgI_2	2.04	0.69	0.59	0.84	66
PEO/TiO_2	3.71	0.75	0.59	1.68	67
PAN/PGE	6.96	0.57	0.65	2.62	68
PVDF/SiO_2	8.32	0.70	0.54	3.22	69
PVDF-HFP/AIN	9.48	0.60	0.68	4.17	70
Liquid electrolyte	7.20	0.75	0.66	3.60	71
PVDF-PAN	6.20	0.74	0.65	3.09	71
PVDF-PAN- Fe_2O_3 3 wt %	9.6	0.75	0.55	3.96	Present work
PVDF-PAN- Fe_2O_3 5 wt %	10.0	0.76	0.56	4.3	Present work
PVDF-PAN- Fe_2O_3 7 wt %	10.4	0.77	0.62	4.9	Present work

Wettability Test

Contact angles are used to predict wettability and adhesion and to indicate monolayer coverage of adsorbed or deposited films. The contact angles measured for PVDF-PAN-Fe_2O_3 (3, 5, 7 wt %) composite membranes are 134.50°, 135.80°, and 136.60° (as shown in Supporting Information Figure S1). Since the contact angles are higher than 120°, the composites are considered to have superhydrophobic nature. Among the composites, the composite having 7 wt % Fe_2O_3 exhibited highest value of 136.60°. This may be due to increase in the surface roughness and the high surface area due to the incorporation of higher proportion of Fe_2O_3.

Photoelectric Performance of DSSC with Composite PVDF-PAN-Fe_2O_3 Polymer Electrolyte

Since the PVDF-PAN-Fe_2O_3 composite fibers are having good ionic conductivity, porosity percentages, and electrolyte uptake, they are considered to be a good quasi solid-state membrane for DSSCs. The *I–V* measurement curves of the DSSCs with the composite of PVDF-PAN-Fe_2O_3 polymer electrolyte were measured under irradiation of 100 mW cm^{-2}. The *I–V* graph showing the photovoltaic performances for DSSCs constructed from the composites and they are presented in Figure 7(a–c). The dark current–voltage characteristic of the composite of PVDF-PAN-Fe_2O_3 polymer electrolyte membranes is presented in Supporting Information Figure S2 and there was no leaking current observed from the cell under the absence of light. The *I–V* parameters for DSSCs such as short circuit photocurrent density (J_{sc}), open circuit voltage (V_{oc}), fill factor (FF), and the overall energy conversion efficiency (η) are presented in Table I. The fabricated DSSCs exhibited higher photovoltaic performance than that of with PVDF-PAN. This shows that the presence of Fe_2O_3 has a major role in increasing the photovoltaic performance. Among the PVDF-PAN-Fe_2O_3 polymer electrolyte, one which is having 7 wt % Fe_2O_3 shows highest photovoltaic efficiency of 4.9%. This may be due to increase in the content of Fe_2O_3 in the membrane which results in higher roughness, amorphous nature, increase in porosity, electrolyte uptake, and ionic conductivity. This photovoltaic efficiency is higher than those reported recently for similar systems, 0.60, 2.04, 1.66 and 2.20, 1.68%.[66–70]

In our earlier study, we reported the photovoltaic efficiency of the liquid electrolyte-based DSSC as 3.60%.[71] This photovoltaic efficiency was compared with that of the DSSC with PVDF-PAN-Fe_2O_3–7% (Table I) and higher efficiency was observed in the later. This concludes that the DSSCs constructed with PVDF-PAN-Fe_2O_3 have higher photovoltaic efficiency than the liquid electrolyte and PVDF-PAN-based DSSCs.

CONCLUSIONS

The PVDF-PAN-Fe_2O_3 nanofibrous membranes were prepared from a solution of PVDF and PAN by incorporating 3%, 5%, and 7% Fe_2O_3 by electrospinning method. The HRSEM showed that the PVDF-PAN-Fe_2O_3 fiber with 7% Fe_2O_3 has 239 nm diameter with three-dimensional interconnected network of regular morphology with large number of voids and cavities. The porosity percentage is 83.7–84.8% and the electrolyte uptake is 562%. The ionic conductivity of PVDF-PAN-Fe_2O_3 fiber with 7% Fe_2O_3 is 6.81×10^{-2} S cm^{-1}. A high contact angle of 136.60° is observed for this composite fiber which shows the superhydrophobic nature of the membrane. The prepared polymer composite membrane was soaked in the electrolyte solution and used as polymer electrolyte. By employing this polymer electrolyte, DSSCs were fabricated successfully and their photovoltaic performances were evaluated. Good solar-to-light electricity conversion efficiency (4.9%) is achieved from the quasi-solid-state solar cell with the electrospun PVDF-PAN-Fe_2O_3 composite membrane electrolyte. The present strategy has a better performance because of the incorporation of Fe_2O_3 nanoparticles in the polymer matrix which increases the porosity and in turn increases electrolyte uptake.

ACKNOWLEDGMENTS

The authors acknowledge AURF, UGC-BSR and DST-PURSE for funding, School of Physics, Alagappa University, Karaikudi for XRD and Central Electro Chemical Research Institute (CECRI), Karaikudi for IV measurements.

REFERENCES

1. Adachi, M.; Murata, Y.; Okada, I.; Yoshikawa, S. *J. Electrochem Soc.* **2003**, *150*, 488.

2. Amadelli, R.; Argazzi, R.; Bignozzi, C. A.; Scandola, F. *J. Am. Chem. Soc.* **1990**, *112*, 7099.
3. A. Formhals U. S. Patent 1,975,504 (**1934**).
4. A. Formhals U. S. Patent 2,160,962 (**1939**).
5. A. Formhals U. S. Patent 2,187,306 (**1940**).
6. A. Formhals U. S. Patent 2,349,950 (**1944**).
7. Armand, M. *Adv. Mater.* **1990**, *2*, 278.
8. Asano, T.; Kubo, T.; Nishikitani, Y. *J. Photoch. Photobiol. A* **2004**, *164*, 111.
9. Bach, U.; Lupo, D.; Comte, P.; Moser, J. E.; Weissortel, F.; Salbeck, J.; Spreitzer, H.; Gratzel, M. *Nature* **1998**, *395*, 583.
10. Baumgarten, P. K. *J. Colloid Interf Sci.* **1971**, *36*, 71.
11. Berry, J. P., (Wirral, GB2) U.S. Patent 4965110 (**1990**).
12. Bornat, A. (Lancashire, GB2) U.S. Patent 4689186 (**1987**).
13. Cao, J. H.; Zhu, B. K.; Xu, Y. Y. *J. Membr. Sci.* **2006**, *281*, 446.
14. Caruso, R. A.; Schattka, J. H.; Greiner, A. *Adv. Mater.* **2001**, *13*, 1577.
15. Wang, P.; Zakeeruddin, S. M.; Moser, J. E.; Nazeeruddin, M. K.; Sekiguchi, T.; Gratzel, M. *Nat. Mater.* **2003**, *2*, 402.
16. Cao, F.; Oskam, G.; Searson, P. C. *J. Phys. Chem.* **1995**, *99*, 17071.
17. Wang, G.; Zhou, X.; Xiao, X. *Mater. Res. Bull.* **2004**, *39*, 2113.
18. Illeperuma, O. A.; Somasundaram, S. *Sol Energ Mater. Sol C.* **2004**, *84*, 117.
19. Kim, Y. J.; Kim, J. H.; Kang, M. S.; Lee, M. J.; Kang, Y. S. *Adv. Mater.* **2004**, *16*, 1753.
20. Kim, J. Y.; Kim, T. H.; Kim, D. Y.; Park, N. G.; Ahn, K. D. *J. Power Sources* **2008**, *175*, 692.
21. Biancardo, M.; West, K.; Krebs, F. C. *J. Photoch Photobiol.* **2007**, *187*, 395.
22. Yangs, H.; Huang, M. *J. Mater. Chem. Phys.* **2008**, *110*, 38.
23. Matsumoto, M.; Miyazaki, H.; Mutsuhito, K. *Solid State Ionics* **1996**, *89*, 263.
24. Chand, S. *J. Mater. Sci.* **2000**, *35*, 1303.
25. Deitzel, J. M.; Kleinmeyer, J.; Harris, D.; Tan, N. C. B. *Polymer* **2001**, *42*, 261.
26. Demir, M. M.; Yilgor, I.; Yilgor, E.; Erman, B. *Polymer* **2002**, *43*, 3303.
27. Dloczik, L.; Ileperuma, O.; Lauermann, I.; Peter, L. M.; Ponomarev, E. A.; Redmond, G.; Shaw, N. J.; Uhlendorf, I. *J. Phys. Chem.* **1997**, *101*, 10281.
28. Doshi, J.; Reneker, D. H. *J Electrostat.* **1995**, *35*, 151.
29. Drozin, V. G. *J. Colloid Sci.* **1955**, *10*, 158.
30. Feng, L.; Li, S.; Li, H.; Zhai, J.; Song, Y.; Jiang, L.; Zhu, D. *Angew. Chem. Int. Edit.* **2002**, *41*, 1221.
31. Gratzel, M. *J. Photochem. Photobiol. A* **2004**, *164*, 3.
32. Hagfeldt, A.; Gratzel, M. *Chem Rev.* **1995**, *95*, 49.
33. Hagfeldt, A.; Gratzel, M. *Accounts Chemical Res.* **2000**, *33*, 269.
34. Hohman, M. M.; Shin, M.; Rutledge, G.; Brenner, M. P. *Phys. Fluids* **2001**, *13*, 2221.
35. Hou, H. Q.; Jun, Z.; Reuning, A.; Schaper, A.; Wendorff, J. H.; Greiner, A. *Macromolecules* **2002**, *35*, 2429.
36. Hu, Y. J.; Chen, B.; Yuan, Y. *J. Cent South Univ. Tech.* **2007**, *14*, 47.
37. Huang, H. T.; Wunder, S. L. *J. Electrochem. Soc.* **2001**, *148*, 279.
38. Huang, Z. M.; Zhang, Y. Z.; Kotaki, M.; Ramakrishna, S. *Compo. Sci. Tech.* **2003**, *63*, 2223.
39. Huynh, W. U.; Dittmer, J. J.; Alivisatos, A. P. *Science* **2002**, *295*, 2425.
40. Lu, Y.; Yu, S. L.; Chai, B. X. *Polymer* **2005**, *46*, 7701.
41. Bottino, A.; Capannelli, G. *Desalination* **2002**,*146*, 35.
42. Xiaochun, C.; Jun, M.; Xuehua, S.; Zhijun, R. *Appl. Surf. Sci.* **2006**, *253*, 2003.
43. Dar-Jong, L.; Cheng-Liang, C.; Fane-Ming, H.; Liao-Ping, C. *Polymer* **2003**, *44*, 413.
44. Jung, H. R.; Ju, D. H.; Lee, W. J.; Zhang, X.; Kotek, R. *Electrochim Acta* **2009**, *54*, 3630.
45. Chung, S. H.; Wang, Y.; Persi, L.; Croce, F.; Greenbaum, S. G.; Scrosati, B.; Plichta, E. *J. Power Sources* **2001**, *97-98*, 644.
46. Beermann, N.; Vayssieres, L.; Lindquist, S. E.; Hagfeldt, A. *J. Electrochem Soc.* **2000**, *147*, 2456.
47. Yang, Y.; Tao J.; Jin X.; Qin Q. *J. Appl. Polym. Sci.* **2011**, *121*, 1566.
48. Choi, Y. J.; Kim, D. W. *Bull. Korean Chem. Soc.* **2011**, *32*, 605.
49. Chuangchote, S.; Sagawa, T.; Yoshikawa S. *Appl. Phys. Lett.* **2008**, *93*, 033310.
50. Miller, E. L.; Paluselli, D.; Marsen, B.; Rocheleau, R. E. *Thin Solid Films* **2004**, *466*, 307.
51. Dghoughi, L.; Elidrissi, B.; Bernede, C.; Addou, M.; Alaoui, L. M.; Regragui, M.; Erguig, H. *Appl Surf Sci.* **2006**, *253*, 1823.
52. Park, Y. J.; Sobahan, K. M. A.; Hwangbo, C. K. *Surf. Coat. Tech.* **2009**, *203*, 2646.
53. Kim, Y. J.; Ahn, C. H.; Lee, M. B.; Choi, M. S. *Mater. Chem. Phys.* **2011**, *127*, 137.
54. Kim, J. R.; Choi, S. W.; Jo, S. M.; Lee, W. S.; Kim, B. C. *J. Electrochem Soc.* **2005**, *152*, 295.
55. Yu, L. Y.; Xu, Z. L.; Shen, H. M.; Yang, H. *J. Membr. Sci.* **2009**, *337*, 257.
56. SathiyaPriya, A. R.; Subramania, A.; Jung, Y. S.; Kim, K. *J. Langmuir* **2008**, *24*, 9816.
57. Asano, T.; Kubo, T.; Nishikitani, Y. *J. Photoch. Photobio A.* **2004**, *164*, 111.
58. Park, S. H.; Won, D. H.; Choi, H. J.; Hwang, W. P.; Jang, S.; Kim, J. H.; Jeong, S. H.; Kim, J. U.; Lee, J. K.; Kim, M. R. *Sol Energ Mater. Sol C.* **2011**, *95*, 296.
59. Chan, C. K.; Peng, H.; Twesten, R. D.; Jarausch, K.; Zhang, X. F.; Cui, Y. *Nano Lett.* **2007**, *106*, 490.
60. Kiriya, D.; Onoe, H.; Ikeda, M.; Hamachi, I.; Takeuchi, S. *Proceedings in MEMS* **2010**, 927.
61. Chen, D.; Wei, W.; Wang, R.; Zhu, J.; Guo, L. *New J. Chem.* **2012**, *36*, 1589.

62. Zeleny, J. *Phys. Rev.* **1914**, *3*, 69.

63. Cavaliere, S.; Salles, V.; Brioude, A.; Lalatonne, Y.; Motte, L.; Monod, P.; Cornu, D.; Miele, P. *J. Nanopart Res.* **2010**, *12*, 2735.

64. Lee, J. K.; Choi, H. J.; Park, S. H.; Won, D. H.; Park, H. W.; Kim, J. H.; Lee, C. J.; Jeong, S. H.; Kim, M. R. *Mol. Cryst. Liq Cryst.* **2010**, *519*, 234.

65. Yang, Y.; Zhang, J.; Zhou, C.; Wu, S.; Xu, S.; Liu, W.; Han, H.; Chen, B.; Zhao, X. Z. *J. Phys. Chem. B* **2008**, *112*, 6594.

66. Bandara, T. M. W. J.; Dissanayake, M. A. K. L.; Mellander, B. E. *Electrochimica Acta* **2010**, *55*, 2044.

67. Singh, P. K.; Bhattacharya, B.; Nagarale, R. K. *J. Appl. Polym. Sci.* **2010**, *118*, 2976.

68. Chan, Y. F.; Wang, C. C.; Chen, C. Y. *J. Mater. Chem. A* **2013**, *1*, 5479.

69. Yang, Y.; Tao, J.; Jin, X.; Qin, Q. *Int. J. Photoenergy* **2011**, *2011*, 1.

70. Huang, K. C.; Chen, P. Y.; Vittal, R.; Ho, K. C. *Sol Energ Mater. Sol C.* **2011**, *95*, 1990.

71. Sethupathy, M.; Pandey, P.; Manisankar, P. *J. Appl. Polym. Sci.* **2014**, *131*, 40022.